Hydrological feedback from projected Earth greening in the 21st century

Jie Wu, Dashan Wang, Laurent Z.X. Li, Zhenzhong Zeng

Sustainable Horizons 1 (2022) 100007

Contents lists available at ScienceDirect

Sustainable Horizons

journal homepage: www.elsevier.com/locate/horiz

Hydrological feedback from projected Earth greening in the 21st century

Jie Wu [a,b], Dashan Wang [a], Laurent Z.X. Li [c], Zhenzhong Zeng [a,*]

[a] School of Environmental Science and Engineering, Southern University of Science and Technology, Shenzhen, China
[b] Department of Geoscience and Natural Resource Management, University of Copenhagen, Copenhagen, Denmark
[c] Laboratoire de Météorologie Dynamique, Centre National de la Recherche Scientifique, Sorbonne Université, Ecole Normale Supérieure, Ecole Polytechnique, Paris, France

ARTICLE INFO

Keywords:
Earth greening
Earth system modelling
Equilibrium
Evapotranspiration
Soil moisture
DDWW paradigm

ABSTRACT

Earth satellites have observed continuous increasing vegetation growth during the past four decades, a phenomenon called Earth greening. Nearly all Earth System Models (ESMs) participating in Coupled Model Intercomparison Project (CMIP) for Intergovernmental Panel on Climate Change (IPCC) project a continuous greening of the planet during the 21st century. To investigate the hydrological feedback from the projected Earth greening, we prescribed the increase in leaf area index (LAI) in the 21st century as projected by CMIP5 ESMs into a state-of-the-art ESM (IPCLCM), and simulated equilibrium climates for current CO_2 and LAI, an increase of CO_2 alone, an increase of LAI alone, and increases of both CO_2 and LAI, respectively. We find that the greening simultaneously intensifies evapotranspiration and precipitation over land. In terms of soil moisture content, the spatial difference between the responses of evapotranspiration and precipitation causes a hydrological response of the "dry gets drier, wet gets wetter" (DDWW) paradigm. Increasing LAI significantly decreases soil moisture content over dry regions, including the Western North America, Southern South America, East Siberia, Central Asia, South Asia, Northern China, Sahel, Southern Africa, and Australia. Over wet regions, such as the Amazon and Congo rainforests, the greening-induced increase of terrestrial evapotranspiration favors more convective precipitation, so that the new equilibrium does not decrease soil moisture content. The DDWW paradigm in terms of *P-ET* response does not hold over wet areas. To mitigate climate change with forestry, policymakers should prevent degradation of existing forests, support afforestation over wet regions, and avoid planting trees in dry regions.

1. Introduction

Earth satellites have observed continuous increasing vegetation growth during the past four decades, a phenomenon called Earth greening (Zhu *et al.*, 2016; Cortés *et al.*, 2021). Vegetation greening feeds back to the climate through biogeochemical and biophysical processes (Piao *et al.*, 2019). The former is widely studied focusing on the impacts on the carbon cycle (Fang *et al.*, 2001; Piao *et al.*, 2009). The latter is the effects on the hydrological cycle and climate, which are caused by the modifications in the land surface biophysical properties, such as albedo, surface roughness, and evapotranspiration (Alkama *et al.*, 2016; Zeng *et al.*, 2017; Lian *et al.*, 2020; Meng *et al.*, 2020; Yu & Diallo, 2021).

Earth System Models (ESMs) are an essential tool to study these feedbacks, as they could couple the vegetation with the atmosphere and the water cycle (Eyring *et al.*, 2016; Sellar *et al.*, 2020). Nearly all ESMs participating in Coupled Model Intercomparison Project (CMIP) for Intergovernmental Panel on Climate Change (IPCC) project a continuous greening of the planet during the 21st century (Mahowald *et al.*, 2015, 2016; Zhao *et al.*, 2020).

The projected Earth greening is supposed to influence the hydrological cycle significantly. As terrestrial evapotranspiration is dominated by vegetation transpiration (more than 60%) (Jasechko *et al.*, 2013; Good *et al.*, 2015), water losses to the atmosphere generally increase with increasing vegetation growth, which has been a dominant driver of increasing global land evapotranspiration during the past 30 years (Zhang *et al.*, 2015; Zeng *et al.*, 2018). Enhanced evapotranspiration (*ET*) accelerates the recycling of atmospheric moisture and eventually affects precipitation. Besides, the projected Earth greening is expected to produce two opposite effects on soil moisture content, the change of which represents the change of background dryness over the region and is of most relevance to agriculture (Robock *et al.*, 2000; Dai *et al.*, 2004; Seneviratne, 2012). On the one hand, Earth greening decreases surface albedo and absorbs more solar radiation, increases canopy conductance and enhances transpiration to favor more precipitation, both of which support persistence of wetness (Bounoua *et al.*, 2000; Buermann *et al.*, 2001; Spracklen *et al.*, 2012). On the other hand, the greater capacity of water loss associated with greening leads to a faster depletion of soil moisture, which is against the persistence of wetness (Pielke *et al.*, 1998; Kim & Wang, 2012).

* Corresponding author.
E-mail address: zengzz@sustech.edu.cn (Z. Zeng).

https://doi.org/10.1016/j.horiz.2022.100007
Received 6 December 2021; Received in revised form 13 January 2022; Accepted 20 January 2022

Several studies have investigated the hydrological feedback from greening, but these researches focused on the past 30 years or limited to a specific region (Li *et al.*, 2018; Zeng *et al.*, 2018; Lian *et al.*, 2020; Yu & Diallo, 2021). To the best of our knowledge, the response of the hydrological cycle to the projected Earth greening in the 21st century is still uncertain. Besides, whether the spatial pattern of the response emerges as a "wet-get-wetter and dry-get-drier" (DDWW) paradigm is under debate. The original DDWW paradigm was proposed from the thermodynamic response of *P-ET* to global warming and was based on oceanic data (Greve *et al.*, 2014; Greve & Seneviratne, 2015). The land surface is dry compared with the ocean surface and gets drier due to global warming (Dai *et al.*, 2004; Feng & Fu, 2013; Cook *et al.*, 2014; Sherwood & Fu, 2014). The overall drying of the land surface is expected to enhance the frequency and severity of droughts that are of devastating impacts on a wide range of socio-economic sectors particularly for regional agriculture (Dai, 2011; Seneviratne, 2012; Trenberth *et al.*, 2013). Currently, the DDWW paradigm has become a common slogan widely used across different disciplines. However, different uses of the terms "wetting" and "drying", as well as the words "wetter" and "drier", yield inconsistencies in the DDWW paradigm (Roth *et al.*, 2021). Recent studies even indicated that the DDWW paradigm does not apply to land surface (Greve *et al.*, 2014; Greve & Seneviratne, 2015), and the land surface will be less arid in a warming future (Roderick *et al.*, 2015). Thus, the tendency of dryness/wetness over land in the future is very uncertain (e.g., Held & Soden, 2006; Milly & Dunne, 2010; Sheffield *et al.*, 2012; Roderick *et al.*, 2015).

In this study, we used a global climate model coupled with a land surface model to investigate the hydrological feedback from the projected greening in the warming future. We simulated four equilibrium climates for different atmospheric CO_2 concentrations and global LAI distribution. Five questions are addressed in our analysis: (1) How does the hydrological cycle (precipitation, evapotranspiration, soil moisture content and *P-ET*) respond to the projected Earth greening in the 21st century?, (2) Will the spatial pattern of the response of soil moisture and *P-ET* emerge as a DDWW paradigm?, (3) Is the greening-induced change in aridity index representative of the greening-induced change in soil moisture content?, (4) What are the mechanisms behind the response of soil moisture content? (5) What are the implications of the greening-induced change in soil moisture content?

2. Materials and methods

2.1. Projected Earth greening in the 21st century

The projected Earth greening in the 21st century was extracted from 27 state-of-the-art ESMs in CMIP5 used for the fifth Assessment Report (AR5) of the IPCC (Taylor *et al.*, 2012; Stocker *et al.*, 2013). Table 1 lists the models and details of their projections of LAI. We examined the model simulations of annual area-weighted average global land LAI for 1982-2099 (Fig. 1a, HISTORICAL run to 2005 and the medium mitigation scenario RCP4.5 from 2006). All ESMs coupled with a dynamic vegetation model show significant greening of land surface for the 21st century. Along with radiative forcing gradually stabilizing till 2100 (Thomson *et al.*, 2011), LAI in all ESMs tends to be stable in the late 21st century (Fig. 1a). The correlation analysis showed that 9 of the 27 ESMs significantly reproduced the historical interannual variability of land LAI between 1982 and 2005 as observed by Advanced Very High Resolution Radiometer (AVHRR) (Zhu *et al.*, 2013). The satellite-observed significant increase of LAI (0.37 m^2 m^{-2} per decade, $P < 0.05$) has also been reproduced by all the 9 ESMs (BNU-ESM, CCSM4, CESM1-BGC, CESM1-CAM5, HadGEM2-CC, HadGEM2-ES, IPSL-CM5A-LR, MIROC-ESM-CHEM and bcc-csm1-1; 0.31 ±0.23 m^2 m^{-2} per decade, $P < 0.05$) (Fig. 1a and Table 1).

The LAI change at pixel (*i, j*) in month *n* in ESM *k* between the early 21st century (2007-2011) and the late 21st century (2095-2099) is estimated as:

$$\Delta LAI_{2100s}(i,j,n,k) = LAI_{ESM\_2100s}(i,j,n,k) - LAI_{ESM\_2010s}(i,j,n,k) \quad (1)$$

where LAI_{ESM_2100s} and LAI_{ESM_2010s} are the ESM-simulated multiyear average monthly LAI for the early 21st century and the late 21st century, respectively. For the late 21st century, LAI at pixel (*i, j*) in month *n* in ESM *k* is:

$$LAI_{2100s}(i,j,n,k) = LAI_{AVHRR\_2010s}(i,j,n) + \Delta LAI_{2100s}(i,j,n,k) \quad (2)$$

where LAI_{AVHRR_2010s} is the satellite observed multiyear (2007-2011) average monthly LAI. The assumption behind the calculation is that ESMs better capture future seasonal changes in LAI, despite their current tendency to overestimate absolute values of LAI (Malhi *et al.*, 2009). We further assume that an ESM can better capture future change in LAI if it has reproduced the satellite-observed historical change in LAI. Thus, in this study, the ensemble average of the calculated LAI of the 9 ESMs illustrated above was used to project Earth greening in the late 21st century.

Fig. 1b displays the projection of Earth greening for the 21st century. Land surface is projected to be much greener in the late 21st century throughout the globe (Fig. 1b and S1). The global enhancement of LAI is 0.21 m^2 m^{-2}, about 14% of current global land LAI. The most pronounced enhancement of LAI occurs over the regions north of 50 degrees during growing seasons (Fig. 1b, c and Figure S1), where vegetation growth gets a direct benefit from surface warming (Zhou *et al.*, 2001; Dass *et al.*, 2015; Zhu *et al.*, 2016). A large enhancement of LAI is also found in China, the United States, Central Africa including the Congo rainforest, and South America excluding the Amazon. This greening trend is attributed to the change in precipitation pattern and the physiological impact of rising CO_2 (Alkama *et al.*, 2014; Dardel *et al.*, 2014). The mechanisms on why and how vegetation responds to climate and CO_2 changes have been investigated in many studies (e.g., Bathiany *et al.*, 2014; Dardel *et al.*, 2014; Dass *et al.*, 2015; Mahowald *et al.*, 2015; Piao *et al.*, 2015; Zhu *et al.*, 2016). Here we focus on how the Earth system will respond to the projected Earth greening in the late 21st century.

2.2. Model simulations

We performed several AMIP-like numerical experiments to investigate the response of hydrological cycle to the projected Earth greening in the late 21st century (Table 2). Experiment 0 is a control experiment to document the climate under current LAI distribution and atmospheric CO_2 concentration (CTRL). Experiments 1-3 are the climates under increasing LAI (SIM_LAI), rising CO_2 (SIM_CO2), and rising both CO_2 and LAI (SIM_ALL), respectively. SIM_LAI – CTRL documents the response of the Earth system to the projected Earth greening. Yet this response neglects the change in water use efficiency due to rising atmospheric CO_2. To investigate the climate response to greening under rising atmospheric CO_2, we analyze the difference between SIM_ALL – CTRL and SIM_CO2 – CTRL. This approach considers not only the land-climate coupling, but also the effect of rising atmospheric CO_2 on water use efficiency. In all experiments, sea surface temperature and sea ice coverage (oceanic boundary condition) are set to climatological seasonal cycle (e.g., Bounoua *et al.*, 2000; Betts *et al.*, 2007; Costa *et al.*, 2007). Land surface boundary condition in each pixel and each plant function type is prescribed with the different climatological monthly varying LAI. All experiments run for 60 years, starting from the same initial condition.

The Earth System Model used to perform the experiments is IPSLCM5A from the Institute Pierre Simon Laplace modeling community (Marti *et al.*, 2010; Dufresne *et al.*, 2013). The model has participated in the CMIP5 used for IPCC AR5. The atmospheric model is the Laboratoire de Météorologie Dynamique atmospheric general circulation model with Zooming capability (Hourdin *et al.*, 2006). The land surface

Table 1
A summary of the Earth System Models used in this study.

model name	modelling center	land model	Resolution (lon×lat)	dynamic LAI	reproduction of historical LAI
bcc-csm1-1	BCC	BCC-AVIM1.	128×64	y	y
bcc-csm-1-m	BCC	BCC-AVIM1.	320×160	y	n
inmcm4	INM	Simple model	180×120	y	n
ACCESS1-0	CSIRO-BOM	MOSES	192×145	n	n
ACCESS1-3	CSIRO-BOM	CABLE	192×145	n	n
BNU-ESM	GCESS	CoLM+BNU-DGVM	128×64	y	y
CCSM4	NCAR	CLM	288×192	y	y
CESM-BGC	NSF-DOE-NCAR	CLM	288×192	y	y
CESM1-CAM5	NSF-DOE-NCAR	CLM	288×192	y	y
CESM1-WACCM	NSF-DOE-NCAR	CLM	144×96	y	n
CanESM2	CCCma	CLASS2.7+CTEM1	128×64	y	n
FIO-ESM	FIO	CLM3	128×64	n	n
GFDL-CM3	NOAA GFDL	LM3	144×90	y	n
GFDL-ESM2G	NOAA GFDL	LM3	144×90	y	n
GFDL-ESM2M	NOAA GFDL	LM3	144×90	y	n
HadGEM2-CC	MOHC	JULES+TRIFFID	192×145	y	y
HadGEM2-ES	MOHC	JULES+TRIFFID	192×145	y	y
IPSL-CM5A-LR	IPSL	ORCHIDEE	96×96	y	y
IPSL-CM5A-MR	IPSL	ORCHIDEE	144×143	y	n
IPSL-CM5B-LR	IPSL	ORCHIDEE	96×96	y	n
MIROC-ESM	MIROC	MATSIRO+SEIB-DGVM	128×64	y	n
MIROC-ESM-CHEM	MIROC	MATSIRO+SEIB-DGVM	128×64	y	y
MIROC5	MIROC	MATSIRO+SEIB-DGVM	256×128	n	n
MPI-ESM-LR	MPI-M	JSBACH+BETHY	192×96	y	n
MPI-ESM-MR	MPI-M	JSBACH+BETHY	192×96	y	n
NorESM1-M	NCC	CLM4	144×96	y	n
NorESM1-ME	NCC	CLM4	144×96	y	n

* The row 'dynamic LAI' shows whether there is any interannual variability of LAI. The row 'reproduction of historical LAI' shows whether there is a significant correlation ($R > 0$, $P < 0.05$) between modelled land LAI (historical run) and observed land LAI (AVHRR LAI3g) from 1982 to 2005.

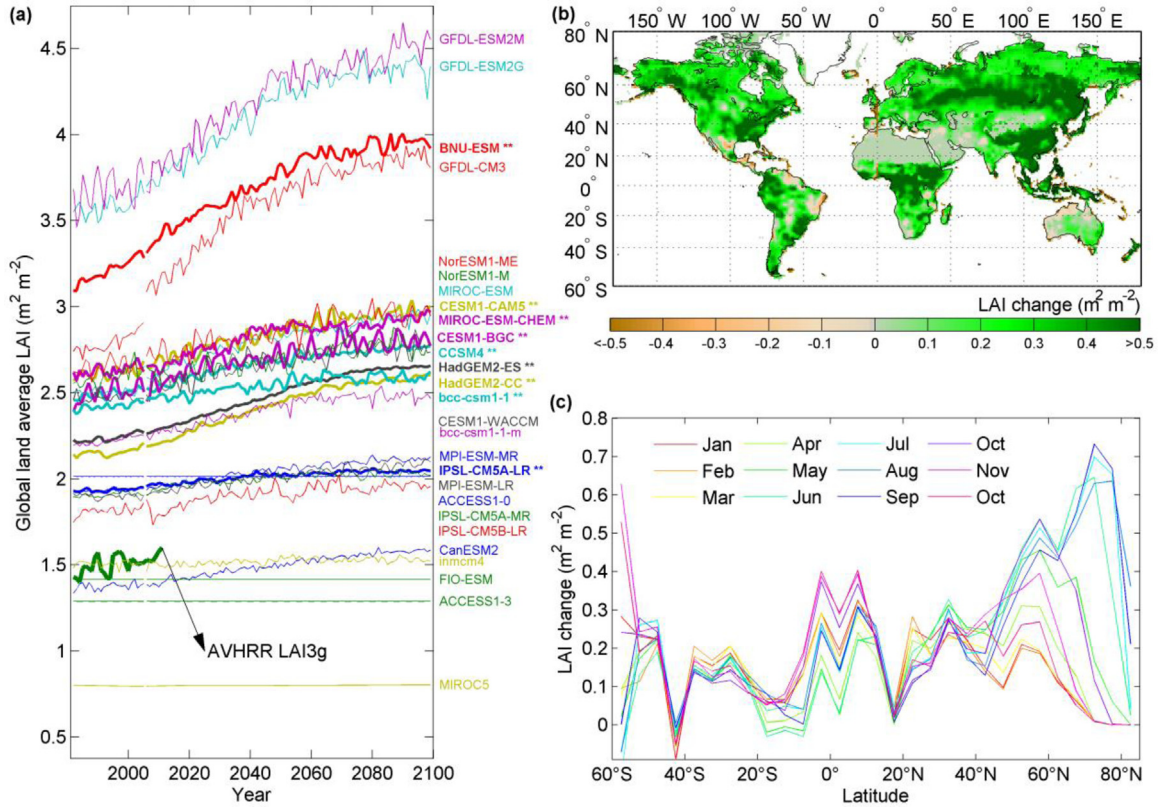

Fig. 1. Projected changes in LAI from the CMIP5 ESMs for 1982 to 2099. (**a**) Interannual variation of global land LAI in each ESMs. LAI during 1982-2005 is derived from the historical run, and that during 2006-2099 from the RCP4.5 run. The bold green line shows the interannual LAI during 1982-2011 as observed from the AVHRR satellites. The bold lines or *** after the model names indicate that the ESM has significantly reproduced the satellite-observed historical change in LAI. (**b**) Spatial pattern of the projected Earth greening in the late 21st century (the change of LAI between the late 21st century (2095-2099) and the early 21st century (2007-2011)). (**c**) Same as (b) but shown at latitude and month spaces.

Table 2
Numerical experiments in this study to quantify the response of Earth system to the projected Earth greening.

Experiment	Simulation	LAI	CO_2
0	CTRL	current	current
1	SIM_LAI	projected	current
2	SIM_CO2	current	projected
3	SIM_ALL	projected	projected

* Current LAI is the multiyear (2007-2011) average monthly LAI as observed from AVHRR. Projected LAI is the multiyear (2095-2099) average monthly LAI as calculated from Eq. (2) using CMIP5 RCP4.5 simulations. Current CO_2 is 390 ppm. Projected CO_2 is 538 ppm in the late 21st century under RCP4.5 scenario.

model is Organising Carbon and Hydrology In Dynamic Ecosystems (ORCHIDEE) (Krinner *et al.*, 2005). ORCHIDEE is proved to be of capacity to simulate terrestrial water cycle well (Piao *et al.*, 2007; Rebel *et al.*, 2012; Mueller & Seneviratne, 2014). In ORCHIDEE, evapotranspiration is modeled as the sum of vegetation transpiration, soil evaporation, interception, and sublimation; the simulation of these processes has considered temperature, radiation, wind speed, specific humidity, vegetation growth activity, and soil moisture deficit (Krinner *et al.*, 2005). As shown in Figure S2, the simulated climatology of precipitation, temperature and evapotranspiration in CTRL are significantly correlated with the observed patterns (R = 0.71, 0.99, 0.83, respectively; all with $P < 0.001$). The spatial resolution is 1.5° latitude × 3.0° longitude and 19 vertical levels, and the temporal resolution is a 1.5 minute time step. All the simulations were performed on the Tianhe supercomputer (TH-1A) in the National Supercomputing Center in Tianjin, China.

2.3. Analysis

We restricted the analysis to the vegetation regions where the multiyear average LAI is larger than 0.1. To ensure that the simulated soil moisture fields are in balance with the climate, we also restricted the analysis to the last 50 years of the simulations, when these experiments reached equilibrium after 10 years (Figure S3) (Seneviratne *et al.*, 2006; Costa *et al.*, 2007). The 50-year-long simulations allow us to quantify unforced internal climate variability and test whether the response is significant from internal variability (two-sample *t*-tests, n = 50) (Swann *et al.*, 2012; Devaraju *et al.*, 2015).

We calculated potential evapotranspiration and aridity index using model outputs. We applied the Penman-Monteith (PM) algorithm to calculate potential evapotranspiration (Penman, 1948). The PM algorithm is generally accepted as the most comprehensive physically based algorithm to model evapotranspiration (Sheffield *et al.*, 2012). The PM equation for actual evapotranspiration is

$$ET = \frac{\Delta}{\Delta + \gamma(1 + r_s/r_a)} Rnet + \frac{\rho c_p / r_a}{\Delta + \gamma(1 + r_s/r_a)} D \tag{3}$$

where ET is actual evapotranspiration (W m^{-2}), $Rnet$ is surface net radiation (W m^{-2}), D is vapour-pressure deficit (Pa), Δ is the slope of the plot of saturated vapour pressure against air temperature (kPa $°C^{-1}$), γ is the psychometric constant (kPa $°C^{-1}$), ρ is the air density (kg m^{-3}), c_p is the specific heat of air at constant pressure (J kg $°C^{-1}$). r_a is aerodynamic resistances (s m^{-1}), and it is controlled by wind speed. r_s is surface resistances (s m^{-1}), and it is the reciprocal of canopy conductance g_c,

$$r_s = g_c^{-1} = \frac{1}{g_{s\max}\beta(w)\frac{1}{k_1/LAI + k_2}} \tag{4}$$

where $g_{s\max}$ is leaf-level maximum conductance, $\beta(w)$ is soil moisture stress scalar, and w is soil moisture content, LAI is leaf area index, k_1 and k_2 are parameters dependent on aerodynamic roughness and vegetation type.

Assuming a zero surface resistance (r_s), the standard PM equation collapses to potential evapotranspiration (Sheffield *et al.*, 2012). It writes as

$$PE = s_1 \frac{\Delta}{\Delta + \gamma} Rnet + s_2 \frac{\gamma}{\Delta + \gamma} 6.43(1 + 0.536U)D \tag{5}$$

where PE is potential evapotranspiration (mm day^{-1}), U is wind speed at 2-meter height (m s^{-1}). The constant s_1 (0.035) changes a unit of W m^{-2} to mm day^{-1}, and the constant s_2 (0.408) changes a unit of MJ m^{-2} day^{-1} into mm day^{-1}. All of Δ, γ, $Rnet$ and D can be calculated from the model outputs of air temperature, humidity, net radiation, and surface pressure.

Aridity index is defined as the ratio of potential evapotranspiration over precipitation (Greve *et al.*, 2014; Greve & Seneviratne, 2015; Lin *et al.*, 2015),

$$AI = \frac{PE}{P} \tag{6}$$

where AI is aridity index, PE is potential evapotranspiration (mm day^{-1}) and P is precipitation (mm day^{-1}).

3. Results

3.1. Change in precipitation and evapotranspiration due to the projected Earth greening

We first investigated the Earth greening induced precipitation and evapotranspiration change by analyzing the difference between SIM_ALL – CTRL and SIM_CO2 – CTRL (see methods). The results show that the projected greening is simulated to increase land surface precipitation, particularly over tropical rainforests and boreal forests (Fig. 2a). A widespread and significant increase of precipitation is also found over Northern Hemisphere mid-high latitudes during MAM (March, April and May) and JJA (June, July and August; Fig. 2b-c).

As for evapotranspiration, both the potential evapotranspiration and actual evapotranspiration are investigated. Following Eq. 5, potential evapotranspiration is controlled by net radiation, air temperature, wind speed, humidity and surface pressure. All these factors are influenced by the greening of the Earth. The results show that the projected greening decreases potential evapotranspiration over a large part of the land surface (Fig. 3), particularly Northern Hemisphere mid-high latitudes during MAM and JJA (Fig. 3b-c). In contrast, the increasing LAI leads to a worldwide spread increase in actual evapotranspiration (Fig. 4). To better separate the direct vegetation feedback and vegetation-soil-hydroclimate feedback, we expanded the actual evapotranspiration to two parts: the biological process of plant transpiration and the physical process of evaporation (the sum of soil evaporation, interception and sublimation). As shown in Figure S4 and S5, plant transpiration sees a worldwide increase in response to the projected greening (Figure S4a), especially over the Northern Hemisphere mid-high latitudes during JJA (Figure S4c). In contrast, the response of evaporation showed regional differences (Figure S5): the greening-induced evaporation increased in most of the Northern Hemisphere and Africa but decreased in the Amazon basin and Australia at the annual scale (Figure S5a).

Several reasons account for the opposite direction of the change in potential evapotranspiration and that in actual evapotranspiration, as a response to the greening of the Earth in the late 21st century. Potential evapotranspiration is based on the assumption of sufficient water supply (mathematically, a zero of surface resistance); namely, this conception neglects the change in the capacity of water loss associated with a change in vegetation growth activity. In fact, increasing LAI decreases surface resistance directly (Eq. 4), leading to a greater capacity of water loss and acceleration of actual evapotranspiration (Eq. 4). As vegetation transpiration dominates evapotranspiration over land (Jasechko *et al.*, 2013; Good *et al.*, 2015), the influence of vegetation growth on terrestrial evapotranspiration is non-neglectable. As shown in Fig. 4, the effect

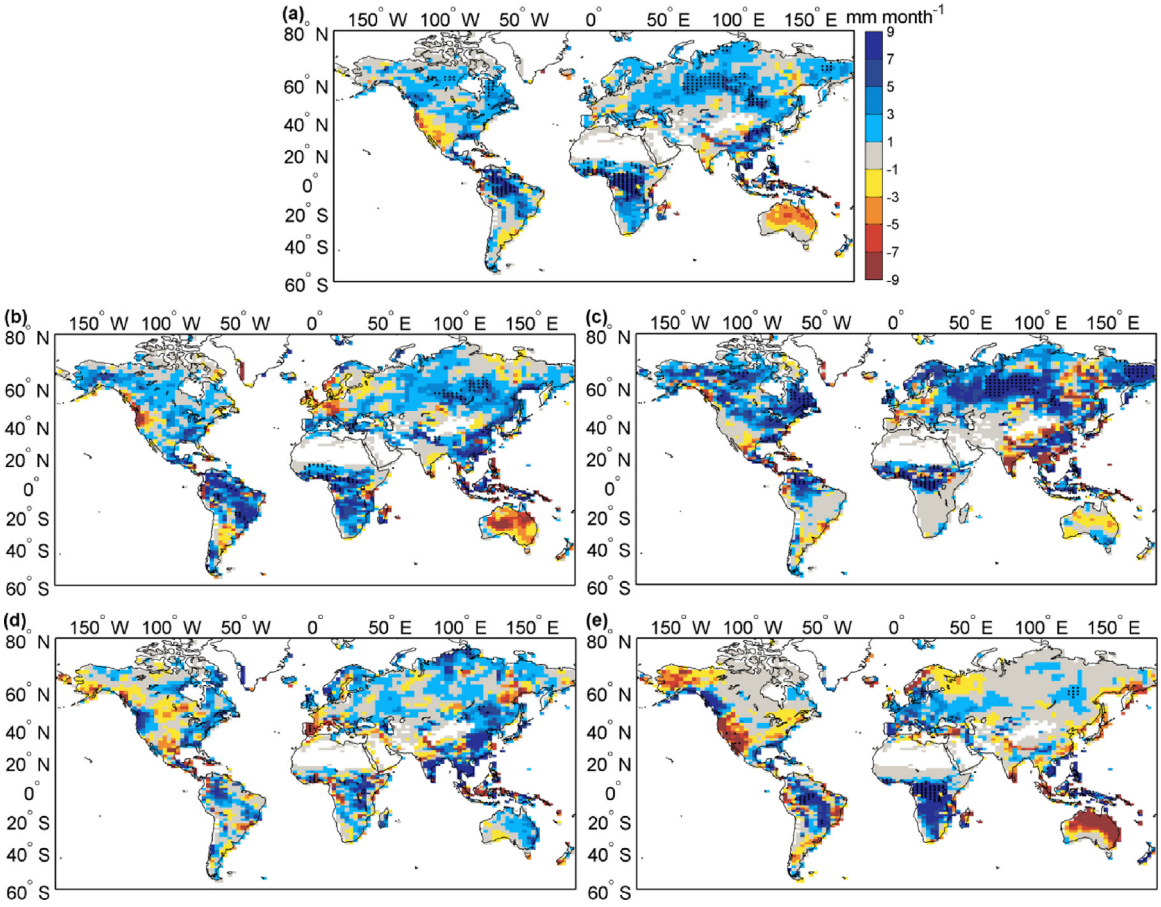

Fig. 2. Response of precipitation to the projected Earth greening in the late 21st century: (a) annual, (c) MAM, (d) JJA, (e) SON, and (f) DJF. The response is calculated as the difference between SIM_ALL – CTRL and SIM_CO2 – CTRL. Dotting indicates significant at $P < 0.05$.

is so strong that increasing LAI leads to a worldwide spread increase in actual evapotranspiration. As a result, first, the increase in evapotranspiration accelerates the moisture cycle and thus increases cloudiness (Figure S6a) and precipitation (Fig. 2). The increase in cloudiness further decreases incoming solar radiation over land. Second, the increase in evapotranspiration leads to an increase in specific humidity (Figure S6b), which decreases the vapor-pressure deficit. Third, the increase in evapotranspiration leads to evaporative cooling that decreases surface air temperature (Figure S6c). Last, increasing LAI increases surface roughness and decreases wind speed (Figure S6d). All of the decreases in solar radiation, vapor-pressure deficit, surface air temperature and wind speed lead to a decrease in potential evapotranspiration (Eq. 5; Fig. 3), which seems to be paradoxical with an increase in actual evapotranspiration, but actually to be a result of the increase in actual evapotranspiration. In conclusion, decreasing potential evapotranspiration provides a strong indication of increasing terrestrial evapotranspiration, which is similar to the pan evapotranspiration paradox (Brutsaert & Parlange, 1998).

3.2. Change in soil moisture content due to the projected Earth greening

We also investigated the Earth greening induced soil moisture change using the same methods. Figure 5a shows that increasing LAI significantly ($P < 0.05$) decreases soil moisture content over the Western North America, Southern South America, East Siberia, Central Asia, South Asia, Northern China, Sahel, Southern Africa and Australia. Meanwhile, an increase of soil moisture content is simulated over the Amazon and Congo rainforest regions. Over other regions, soil moisture content does not change with the greening (Fig. 5a). Interestingly, it seems that, over almost all arid regions (aridity index > 2, see Fig. 2b), an increase of LAI leads to a reduction in soil moisture content (Fig. 1b, 5a, b).

The spatial patterns of the Earth greening induced soil moisture change in the four seasons (Fig. 5c-f) are similar to that at the annual scale (Fig. 5a). Over South Asia, Southern China and Sahel, the most widespread and robust reduction in soil moisture occurs in boreal spring (MAM; Fig. 5c); over the high northern latitudes, Central North America and Central Asia, that occurs in boreal summer (JJA; Fig. 5d); over the Western United States, and Southern Africa, that occurs in boreal Autumn (SON: September, October and November; Fig. 5e); and over Eastern China and Australia, that occurs in boreal winter (DJF: December, January, and February; Fig. 5f). It seems that the most substantial reduction in soil moisture content occurs in the season when it is relatively arid (Fig. 5c-f, and S7). Taking the Sahel as an example, during the dry seasons (MAM and DJF), soil moisture content significantly and strongly decreases; but during the wet seasons (JJA and SON), soil moisture content only slightly decreases, although LAI increases as much as that in the dry seasons (Fig. 5c-f, Figure S1 and S7). Due to soil moisture memory (Dirmeyer *et al.*, 2009; Rahman *et al.*, 2015), soil moisture change in one season also leads to a change of soil moisture in other seasons. As a result, increasing LAI leads to an annual reduction in soil moisture content over those arid and seasonal arid regions (Fig. 5).

We then investigated the effects of increasing LAI and rising CO_2 on soil moisture content separately. Compared to CTRL, the increase of LAI alone significantly decreases soil moisture content over those arid and seasonal arid regions (SIM_LAI; Fig. 6a). The spatial pattern is almost the same as the result having considered the effect of rising atmospheric CO_2 (Fig. 5a), indicating a weak influence of rising atmospheric CO_2. On the one hand, rising CO_2 tends to reduce the density of stomatal pores in leaves and thus enhance water use efficiency (de Boer *et*

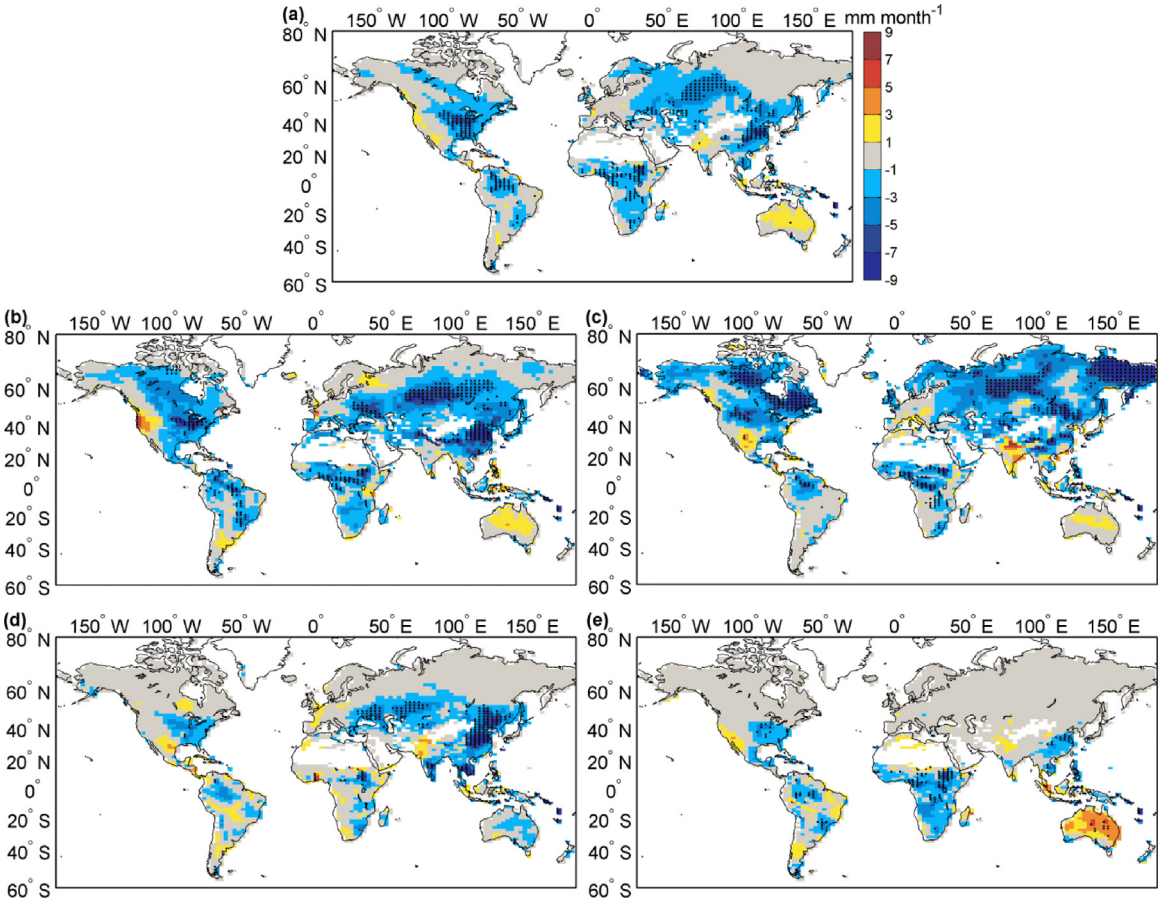

Fig. 3. Response of potential evapotranspiration to the projected Earth greening in the late 21st century: (a) annual, (c) MAM, (d) JJA, (e) SON, and (f) DJF. The response is calculated as the difference between SIM_ALL – CTRL and SIM_CO2 – CTRL. Dotting indicates significant at $P < 0.05$.

al., 2011; Farrior *et al.*, 2015; Schimel *et al.*, 2015). This effect is likely to increase soil moisture content. On the other hand, radiative forcing caused by rising CO_2 increases evaporation capacity. This effect is likely to decrease soil moisture content. As a result, these two opposite effects cancel out each other at most regions (SIM_CO2 – CTRL; Fig. 6b). Fig. 6c demonstrates that the response of soil moisture content to the projected increasing LAI and rising CO_2 in the late 21st century (SIM_ALL – CTRL) is dominated by the effect of increasing LAI (Fig. 6a).

In short, dry lands (defined in terms of the aridity index) get drier (defined in terms of the soil moisture) due to the projected Earth greening in the late 21st century, supporting the DDWW paradigm.

3.3. *Change in* P-ET *and aridity index due to the projected Earth greening*

The original DDWW paradigm was proposed from the thermodynamic response of *P-ET* to global warming, so we also treated *P-ET* as a metric and investigated its response to the projected greening. As shown in Fig. 7, the increase of *P-ET* mainly occurs over the Amazon and Congo rainforests, accounting for only a tiny proportion of wet land areas. For most wet regions such as the boreal forests, the greening-induced *P-ET* decreased. It seems that the DDWW paradigm in terms of *P-ET* does not hold.

Apart from soil moisture content, the aridity index is widely used to characterize background dryness. To verify whether the greening-induced change in aridity index is representative of the change in soil moisture, here we investigated the change in aridity index due to the projected Earth greening. As the projected Earth greening is simulated to reduce soil moisture content over a large part of dry lands (Fig. 5), we expected an increase of aridity index over these regions. However, conversely, the aridity index decreased over many regions, including Central United States, Central Asia, Northern China, Sahel, Southern Africa, and the Amazon (Fig. 8a). At seasonal scale, a significant decrease of aridity index is found over Northern Hemisphere mid-high latitudes during MAM and JJA (Fig. 8b-c). Thus, it is obvious that the change in aridity index is not representative of the response of soil moisture to the greening.

We tried to investigate why the aridity index decreases with the greening of land surface, and why it is not representative of the change in background dryness. Background dryness depends on not only precipitation, but also how fast water would evaporate (Sherwood & Fu, 2014). As for aridity index, the latter is measured with potential evapotranspiration (Eq. 6). As mentioned above, potential evapotranspiration decreases (Fig. 3) and precipitation increases (Fig. 2) over a large part of land surface, which explains the decrease of aridity index as a response to the projected Earth greening in the 21st century (Fig. 8). In addition, as discussed in section 3.1, decreasing potential evapotranspiration provides a strong indication of increasing terrestrial evapotranspiration. Namely, the change in potential evapotranspiration fails to characterize the change in how fast water would evaporate. Therefore, it is no doubt that the change in aridity index is not representative of the change in background dryness in a greening future.

4. Discussions

4.1. *Mechanisms on the response of soil moisture content*

The greening of the Earth increases the capacity of water loss to the atmosphere by decreasing surface resistance (Eq. 4) (Bounoua *et al.*,

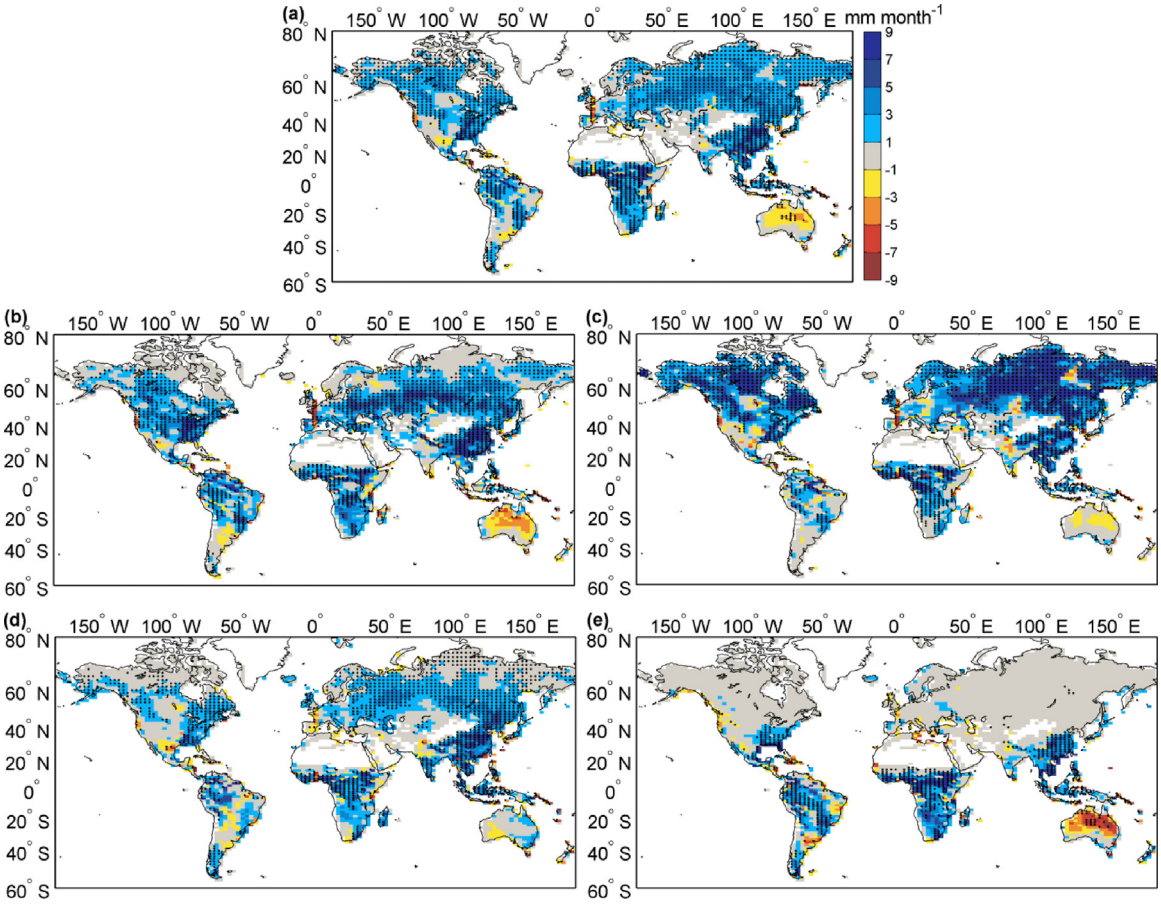

Fig. 4. Response of actual evapotranspiration to the projected Earth greening in the late 21st century: (a) annual, (c) MAM, (d) JJA, (e) SON, and (f) DJF. The response is calculated as the difference between SIM_ALL – CTRL and SIM_CO2 – CTRL. Dotting indicates significant at $P < 0.05$.

2000; Buermann *et al.*, 2001). The greater evapotranspiration capacity breaks the equilibrium between water supply (precipitation) and water demand (evapotranspiration capacity), and the hydrological system adjusts itself to reach a new equilibrium. Given the same soil moisture content, the greater evapotranspiration capacity makes land surface evaporate terrestrial water faster (Eq. 3) and results in a widespread increase of terrestrial evapotranspiration (Fig. 4). If the increase of evapotranspiration does not favor more local precipitation, soil moisture content reduces, and the depletion of soil moisture, in turn, constrains evapotranspiration (Eq. 4). In this situation, it is the reduction in soil moisture content that pulls back the system to the original equilibrium. This situation is found over dry regions where precipitation is not maintained by local recycling water, including the Western United States, Southern South America, East Siberia, Central Asia, India, and Australia (Fig. 2, 4 and 5).

The other situation is that increasing evapotranspiration favors more precipitation, as found over wet regions (Fig. 2). Increasing evapotranspiration adds water into the atmosphere. As the atmosphere cannot continuously hold this increasing water, precipitation increases. The question is where to rain. According to the planetary boundary layer (PBL) theory, PBL is shallowest over wet, vegetated surface and deepest over dry, bare land (Segal *et al.*, 1989; Hohenegger *et al.*, 2009; Rihani *et al.*, 2015). As shown in Figure S8a, the boundary layer height decreased in wet regions in response to the projected greening. There is an immense amount of moist static energy (MSE) over moist vegetation. A shallower PBL with bigger MSE implies a bigger MSE per unit of PBL, which is supportive to an increase of potential for convective development, moist convection, and moisture convergence (Clark & Arritt, 1995; Segal *et al.*, 1995; Betts *et al.*, 1996; De Ridder, 1997; Hohenegger *et al.*, 2009). In return, the increase of moisture convergence boosts convective activity, leading to positive feedback of moisture recycling. Consequently, the greening strengthens the positive moisture-precipitation feedback over moist vegetation (Figure S8b). As a result, our model simulations show that increasing LAI significantly increases precipitation over boreal forests during growing seasons and over tropical rainforests (Fig. 2). The increase in precipitation is even more than the increase in evapotranspiration over the Amazon and Congo rainforests (Fig. 7). In the new equilibrium for the moist vegetated surface, the greening accelerates moisture recycling by altogether increasing evapotranspiration and precipitation, and does not change soil moisture content (Fig. 2, 4, and 5).

Therefore, the change in soil moisture content is a result of the conflict between water supply (precipitation) and water demand (evapotranspiration capacity). Over wet lands, a greater capacity of water loss to the atmosphere associated with greening strengthens the positive moisture-precipitation feedback. It increases both evapotranspiration and precipitation, and does not decrease soil moisture content (wet gets wetter). However, over dry lands, the greater evapotranspiration capacity cannot favor more precipitation and directly decreases soil moisture content (dry gets drier). Then, the spatial pattern of the greening-induced change in soil moisture content emerges as a DDWW paradigm.

4.2. Contribution to DDWW paradigm

Many studies investigated whether DDWW is valid in a warming future (e.g., Held & Soden, 2006; Chou *et al.*, 2009; Seager & Vecchi, 2010; Feng & Fu, 2013; Cook *et al.*, 2014; Greve *et al.*, 2014; Greve & Seneviratne, 2015; Roderick *et al.*, 2015). Most studies support the DDWW paradigm, but recent studies suggest that change in aridity index un-

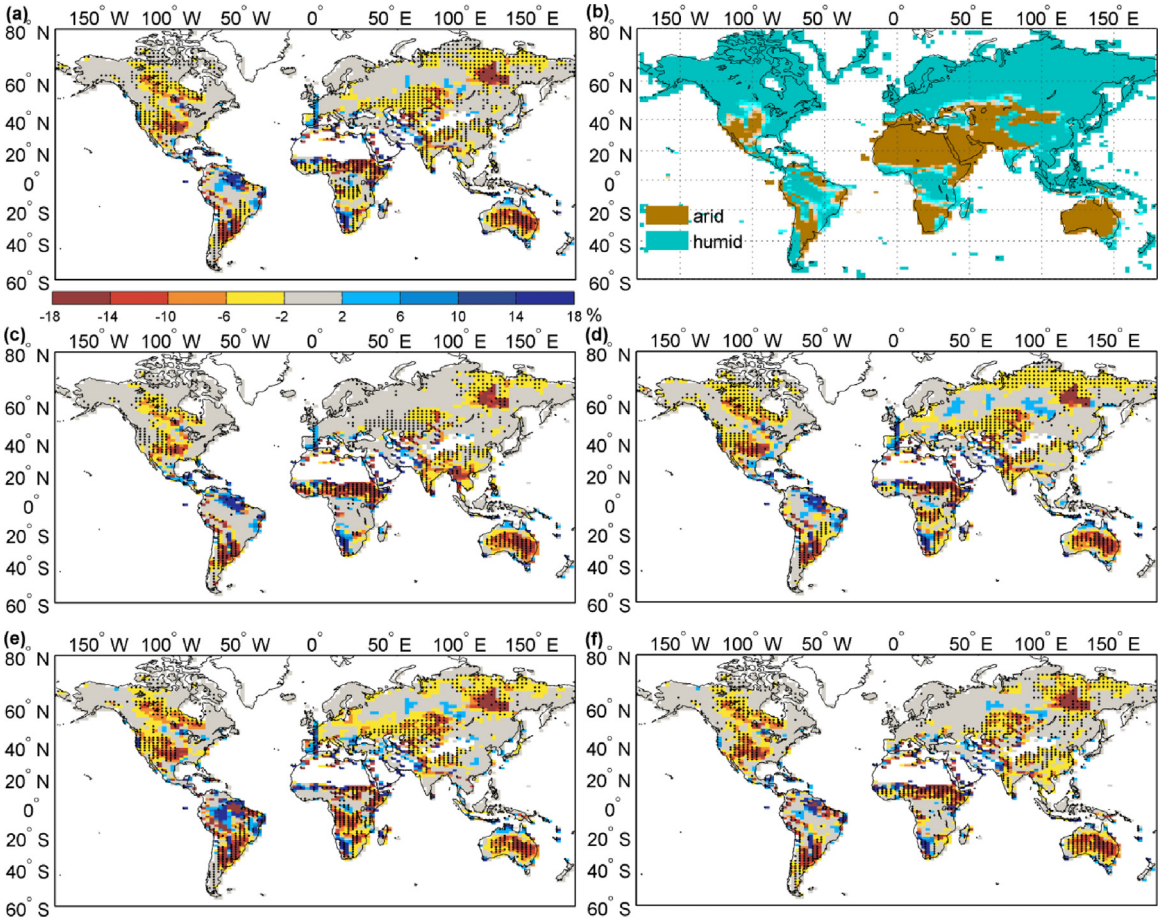

Fig. 5. Response of soil moisture content to the projected Earth greening in the late 21st century: (a) annual, (c) MAM, (d) JJA, (e) SON, and (f) DJF. The response is calculated as the difference between SIM_ALL – CTRL and SIM_CO2 – CTRL. Dotting indicates significant at $P < 0.05$. (**b**) Spatial pattern of arid (aridity index > 2) and humid (aridity index < 2) regions in the control experiment.

der global warming does not follow the DDWW paradigm over land (Greve *et al.*, 2014; Greve & Seneviratne, 2015; Roderick *et al.*, 2015). The debate is mainly caused by the the limited knowledge on evapotranspiration. Sheffield *et al.*, (2012) has pointed out that the widely used temperature-based algorithm to estimate potential evapotranspiration overestimates the drying trend under global warming. The PM-based potential evapotranspiration algorithm (Eq. 5) is the most widely used algorithm to estimate potential evapotranspiration and then aridity index (Sheffield *et al.*, 2012; Greve *et al.*, 2014; Greve & Seneviratne, 2015; Roderick *et al.*, 2015). The algorithm considers net radiation, temperature, humidity and wind speed (Eq. 5) but neglects the evapotranspiration capacity associated with vegetation growth. Nearly all these studies neglected the feedback of the greening of the Earth, which is induced by rising atmospheric CO_2 concentration and its derived climate change (Mahowald *et al.*, 2015, 2016) (Fig. 1 and S1).

Similar to the pan evapotranspiration paradox (Brutsaert & Parlange, 1998), we found that the greening-induced change in potential evapotranspiration is in the opposite direction of the greening-induced change in actual evapotranspiration. The projected Earth greening increases canopy conductance, decreases surface resistance and thus significantly increases actual evapotranspiration (Fig. 4). The increase in evapotranspiration increases precipitation, cools land surface, and decreases net radiation by altering clouds. In addition, increasing LAI slows down wind speed. All these factors contribute to a decrease of the PM-based potential evapotranspiration (Fig. 3). The increase in precipitation and the decrease in potential evapotranspiration result in a decrease of aridity index over most of land surface (Fig. 8), which is in contrary to the change in soil moisture content (Fig. 5). Because the change in potential evapotranspiration is not representative of the terrestrial evapotranspiration, the change in aridity index is also not representative of the change in background dryness in a greening and warming future.

Our model simulations (SIM_CO2) show that the rising atmospheric CO_2 concentration itself does not change soil moisture content over most of land surface (Fig. 6b). By contrast, the simulations forced by the projected Earth greening in the late 21st century (SIM_LAI, SIM_ALL) show a significant decrease in soil moisture content over dry lands particularly during dry seasons (Fig. 6a and c). It indicates "dry gets drier". Over wet lands, the greening strengthens the positive moisture-precipitation feedback by increases in both evapotranspiration and precipitation (Fig. 2 and 4), keeping soil moisture content at a relatively constant level (Fig. 5). That implies "wet gets wetter". In summary, rising CO_2 alone does not cause a hydrological response of DDWW paradigm, but the projected Earth greening in the late 21st century does.

4.3. Implication for carbon cycle and forestry policy

In response to a rise of atmospheric CO_2 concentration, plants reduce diffusive stomatal conductance of their leaves and thus the maximal leaf-level maximum conductance $g_{s\,\max}$ (de Boer *et al.*, 2011; Lammertsma *et al.*, 2011). With a reduction of $g_{s\,\max}$, plants minimize transpirational water loss and maximize assimilation rate. That is an enhancement of water use efficiency ($WUE = {}^{GPP}/_{ET}$, where WUE is water use efficiency, GPP gross primary production). The enhancement of WUE indicates that the same amount of water can be used to trade for more carbon (Jackson *et al.*, 2005). The maximum amount of renewable wa-

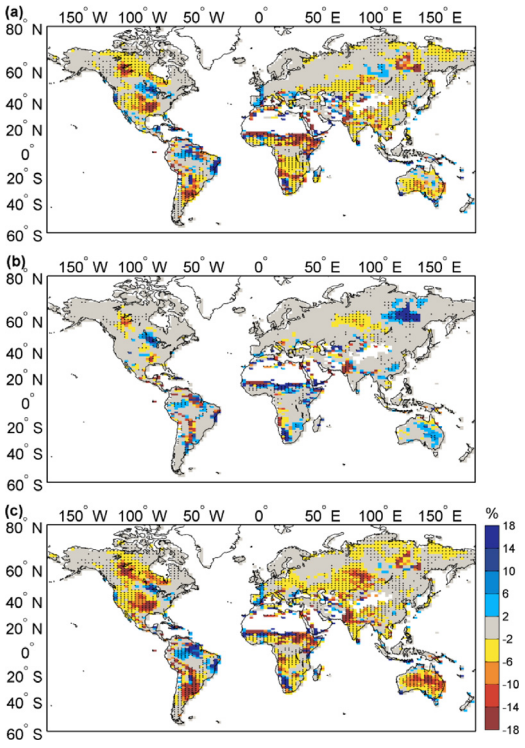

Fig. 6. Spatial patterns of the change in soil moisture content in (a) SIM_LAI – CTRL, (b) SIM_CO2 – CTRL, and (c) SIM_ALL – CTRL. Dotting indicates significant at P < 0.05.

ter for plants over dry lands is precipitation (Zeng *et al.*, 2013). Thus, the optimization of the usage of precipitation leads to a greening over dry lands (Bathiany *et al.*, 2014; Farquhar, 1997; Donohue *et al.*, 2013; Farrior *et al.*, 2015).

The coexistence of greening and drying over dry lands has implication for the global carbon cycle. The carbon pool in dryland biomes is tremendous as dryland ecosystems cover 45% of the Earth's land surface (Grace *et al.*, 2006, Poulter *et al.*, 2014). The large interannual variation of precipitation over dry lands leads dryland ecosystems to be one of the key drivers of the global carbon cycle interannual variability (Poulter *et al.*, 2014). On the one hand, as the same precipitation can trade for more carbon under rising WUE, the same interannual variation of precipitation results in a more significant interannual variability of carbon cycle over dry regions ($GPP = WUE \times P$, where P is precipitation to trade for carbon; it is representative for greening). On the other hand, the drying of land surface indicates that vegetation growth is more sensitive to precipitation. As a result, the global carbon cycle interannual variability is expected to increase due to the coexistence of greening and drying over dry lands.

Forestry policymakers tend to support the policies that are favorable to plant more trees, considering the valuable ecological, economic, social and aesthetic services provided by forests (Bonan, 2008). Afforestation also helps slow down the increase of CO_2 concentration and contributes to climate change mitigation (Robert *et al.*, 2008). However, forestry policymakers rarely took the biophysical feedback of afforestation into consideration. A comprehensive, global view of the feedback sheds some light on the effects of forestry activities. The different responses of soil moisture to increasing LAI between dry and wet lands help to optimize the location and species of afforestation.

Over wet lands, the projected greening strengthens the positive moisture-precipitation feedback, favors more precipitation and even induces more water yield (Fig. 2 and 7). Thus forestry policymakers should

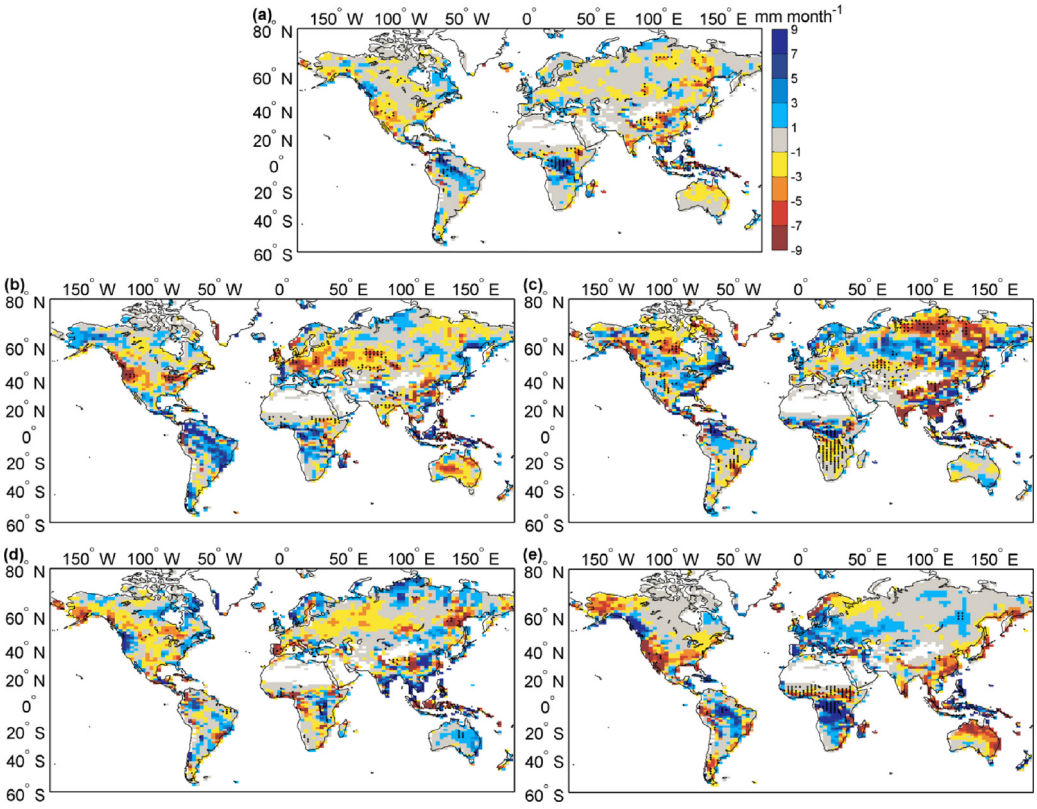

Fig. 7. Response of *P-ET* (i.e. precipitation minus evapotranspiration) to the projected Earth greening in the late 21st century: (a) annual, (c) MAM, (d) JJA, (e) SON, and (f) DJF. The response is calculated as the difference between SIM_ALL – CTRL and SIM_CO2 – CTRL. Dotting indicates significant at P < 0.05.

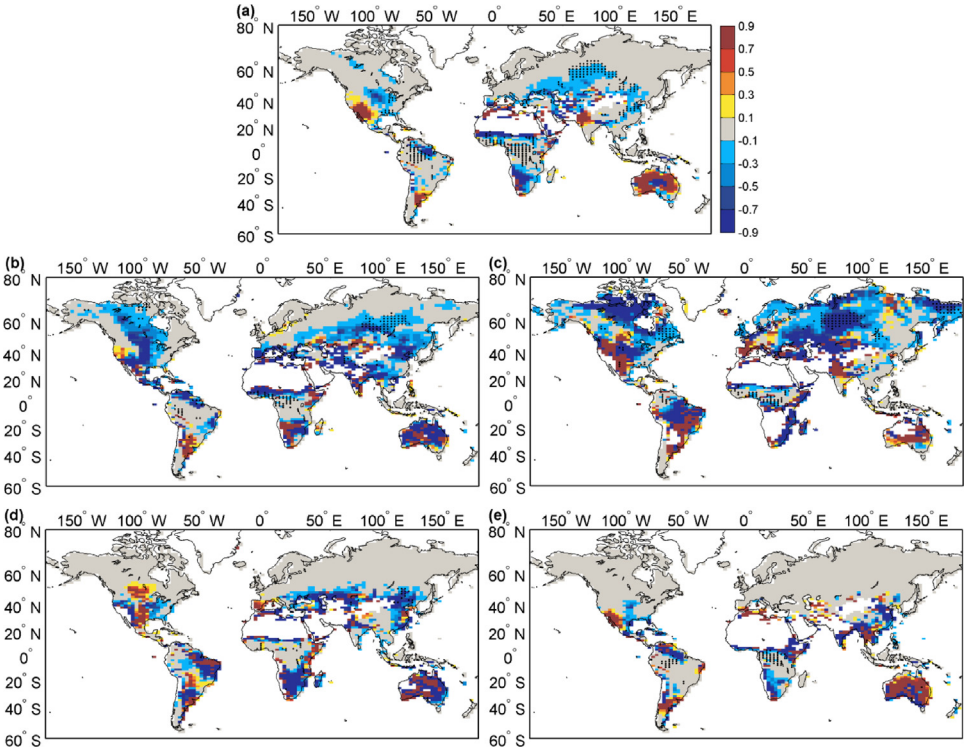

Fig. 8. Response of aridity index to the projected Earth greening in the late 21st century: (a) annual, (c) MAM, (d) JJA, (e) SON, and (f) DJF. The response is calculated as the difference between SIM_ALL – CTRL and SIM_CO2 – CTRL. Dotting indicates significant at $P < 0.05$.

prevent the degradation of existing forests and support more afforestation over these regions. Over dry lands, the greening reduces soil moisture content, resulting in a higher sensitivity of dryland ecosystem to meteorological drought. This indicates that even a slight decrease in precipitation may cause a severe drought event. With the severe drought, trees die and carbon sequestration by afforestation releases back to the atmosphere. In addition, greening also decreases water yield (Farley *et al.*, 2005; Fig. 7), indicating a decrease of renewable water for human society. Thus forestry policymakers should avoid planting trees over dry lands, and support a recreation of natural ecosystems adapted to local environments. The Chinese government used to invest vast amounts of money in planting trees over dry lands to alleviate land degradation, which in return decreased the soil moisture content there and further increased environmental degradation (Cao, 2008; Cao *et al.*, 2010). Currently, these efforts have been changed to "planting trees only when it is suitable", which has led to significant increases in leaf area and carbon sequestration (Chen et al., 2019).

4.4. Caveats and limitations

There are some uncertainties associated with the experiment setup, the model representation of soil moisture stress on vegetation, and the number of ESMs involved. First, our experiments are initiated from the historical climate and plant functional types. For example, SST and sea ice coverage (oceanic boundary condition) were constrained from the historical observation data. This is unrealistic to some degree when targeting the future since vegetation's hydrological feedback depends on background states such as climate, plant functional type, and vegetation phenology (Dirmeyer *et al.*, 2021; Notaro *et al.*, 2020). However, large uncertainty remains in the future SST and oceanic boundary condition, which would induce additional uncertainties. So, we took the historical climate and plant functional types as an alternative, which also helps to simplify the interpretation.

Besides, the model representation of the soil moisture stress on vegetation would bring uncertainties. In many land surface models, the regulation of stomatal conductance is represented as a function of soil moisture content. The simple generic function is generally expressed using volumetric water content, the so-called 'beta' function (Harper *et al.*, 2021). The land surface model ORCHIDEE also includes the 'beta' function to represent the vertical soil flow in its 11-layer soil diffusion model (Traore *et al.*, 2014). However, the parameters representing plant and soil hydraulic properties vary between ecosystem types and may change over time, so applying one function for all plants may lead to errors. Another uncertainty comes from the fixed soil depth of 2 m everywhere in the 11-layer module in ORCHIDEE, limiting access to deep soil moisture.

In addition, analyzing a single Earth system model is a limitation of the current study. Although ESMs represent the highest level of human climate simulation, these state-of-the-art ESMs are still subject to considerable uncertainties, especially the various parameterization schemes within them. Different treatments of the parameterization schemes of cumulus convection, turbulence, radiation, cloud microphysics, and land surface processes in ESMs may cause differences in model simulation results. As a result, the hydroclimate feedbacks of vegetation may vary a lot by the model. To eliminate as much uncertainty as possible caused by a single model, we thoroughly assessed the capability of IPSLCM ESM to accurately simulate the response of land surface evapotranspiration to changes in vegetation growth activity, namely, the sensitivity of ET to LAI ($\partial ET/\partial LAI$) in the model. Previous studies have shown that the $\partial ET/\partial LAI$ simulated by the IPSLCM ESM is 0.32 ± 0.01mm/day, which is consistent with the observation-based results (Zeng *et al.*, 2017). Therefore, IPSLCM is considered to have the ability to simulate vegetation-climate feedback.

5. Conclusion

The hydrological feedback from Earth greening is often investigated focusing on the past greening or being limited to a specific region. Less attention has been paid to the feedbacks of projected Earth greening in the 21st century. The greater capacity of water loss associated with the greening of the Earth could directly change soil moisture content via an adjustment of the equilibrium between water supply and demand of the terrestrial hydrological cycle. Our numerical experiments clearly show that rising CO_2 alone does not cause a hydrological response of "dry gets drier, wet gets wetter" paradigm, but increasing LAI does. The pro-

jected Earth greening in the late 21st century significantly decreases soil moisture content over dry lands, including the Western North America, Southern South America, East Siberia, Central Asia, South Asia, Northern China, Sahel, Southern Africa and Australia. Over wet lands, the greening-induced increase of terrestrial evapotranspiration favors more convective precipitation, so that the equilibrium is established with altogether acceleration of precipitation and evapotranspiration under a greening future.

Declaration of Competing Interest

The authors declare that they have no known competing financial interests or personal relationships that could have appeared to influence the work reported in this paper.

Author Biographies

Acknowledgements

We are grateful to the World Climate Research Programme Working Group on Coupled Modelling and the climate modeling groups listed in Table 1 for the model outputs of CMIP5. This study was supported by the National Natural Science Foundation of China (42071022) and the startup fund provided by the Southern University of Science and Technology (29/Y01296122). The authors thank the National Supercomputing Center in Tianjin and the Center for Computational Science and Engineering at Southern University of Science and Technology for providing computing resources.

Supplementary materials

Supplementary material associated with this article can be found, in the online version, at doi:10.1016/j.horiz.2022.100007.

References

Alkama, R., Cescatti, A., 2016. Biophysical climate impacts of recent changes in global forest cover. Science 351, 600–604.
Bathiany, S, Claussen, M, Brovkin, V, 2014. CO_2-induced Sahel greening in three CMIP5 Earth System Models. J. Clim. 27, 7163–7184.
Betts, AK, Ball, JH, Beljaars, ACM, Miller, MJ, Viterbo, PA, 1996. The land surface-atmosphere interaction: A review based on observational and global modeling perspectives. J. Geophys. Res. Atmos. 101, 7209–7225.
Betts, RA, Boucher, O, Collins, M, et al., 2007. Projected increase in continental runoff due to plant responses to increasing carbon dioxide. Nature 448, 1037–1041.
Bonan, GB, 2008. Forests and climate change: Forcings, feedbacks, and the climate benefits of forests. Science 320, 1444–1449.
Bounoua, L, Collatz, GJ, Los, SO, Sellers, PJ, Dazlich, DA, Tucker, CJ, Randall, DA, 2000. Sensitivity of climate to changes in NDVI. J. Clim. 13, 2277–2292.
Brutsaert, W, Parlange, M, 1998. Hydrologic cycle explains the evaporation paradox. Nature 396 30-30.
Buermann, W, Dong, J, Zeng, X, Myneni, RB, Dickinson, RE, 2001. Evaluation of the utility of satellite-based begetation leaf area index data for climate simulations. J. Clim. 14, 3536–3550.
Cao, S, 2008. Why large-scale afforestation efforts in China have failed to solve the sesertification problem. Environ. Sci. Technol. 42, 1826–1831.
Cao, S, Tian, T, Chen, L, Dong, X, Yu, X, Wang, G, 2010. Damage caused to the environment by reforestation policies in arid and semi-arid areas of China. Ambio 39, 279–283.
Chen, C., et al., 2019. China and India lead in the greening of the world through land-use management. Nat. Sustain. 2, 122.
Chou, C, Neelin, JD, Chen, CA, Tu, JY, 2009. Evaluating the “rich-get-richer” mechanism in tropical precipitation change under global warming. J. Clim. 22, 1982–2005.
Clark, CA, Arritt, PW, 1995. Numerical simulations of the effect of soil moisture and vegetation cover on the development of deep convection. J. Appl. Meteorol. 34, 2029–2045.
Cook, B, Smerdon, J, Seager, R, Coats, S, 2014. Global warming and 21st century drying. Clim. Dyn. 43, 2607–2627.
Cortés, J, Mahecha, M D, Reichstein, M, Myneni, RB, Chen, C, Brenning, A, 2021. Where are global vegetation greening and browning trends significant? Geophys. Res. Lett. 48 (6) e2020GL091496.
Costa, MH, Yanagi, SNM, Souza, PJOP, Ribeiro, A, Rocha, EJP, 2007. Climate change in Amazonia caused by soybean cropland expansion, as compared to caused by pastureland expansion. Geophys. Res. Lett. 34, L07706.
Dai, A, 2011. Drought under global warming: A review. Wiley Interdiscip. Rev. Clim. Change 2, 45–65.
Dai, A, Trenberth, KE, Qian, T, 2004. A global dataset of Palmer Drought Severity Index for 1870–2002: Relationship with soil moisture and effects of surface warming. J. Hydrometeorol. 5, 1117–1130.
Dardel, C, Kergoat, L, Hiernaux, P, Mougin, E, Grippa, M, Tucker, CJ, 2014. Re-greening Sahel: 30 years of remote sensing data and field observations (Mali, Niger). Remote Sens. Environ. 140, 350–364.
Dass, P, Rawlins, MA, Kimball, JS, Kim, Y, 2015. Environmental controls on the greening of terrestrial vegetation across northern Eurasia. Biogeosciences Discuss 12, 9121–9162.
De Boer, HJ, Lammertsma, EI, Wagner-Cremer, F, Dilcher, DL, Wassen, MJ, Dekker, SC, 2011. Climate forcing due to optimization of maximal leaf conductance in subtropical vegetation under rising CO_2. Proc. Natl. Acad. Sci. 108, 4041–4046.
De Ridder, K, 1997. Land surface processes and the potential for convective precipitation. J. Geophys. Res. 102, 30085.
Devaraju, N, Bala, G, Modak, A, 2015. Effects of large-scale deforestation on precipitation in the monsoon regions: Remote versus local effects. Proc. Natl. Acad. Sci., 201423439.
Dirmeyer, PA, Schlosser, CA, Brubaker, KL, 2009. Precipitation, recycling, and land memory: An integrated analysis. J. Hydrometeorol. 10, 278–288.
Dirmeyer, PA, Huang, K, Lydeen, N, Manthos, Z.H, Knapp, S, Hay-Chapman, FM, 2021. Projected hydroclimate changes driven by carbon dioxide trends and vegetation modeling in CMIP6. Earth and Space Science Open Archive 34. doi:10.1002/essoar.10506162.1.
Donohue, RJ, Roderick, ML, Mcvicar, TR, Farquhar, GD, 2013. Impact of CO_2 fertilization on maximum foliage cover across the globe’s warm, arid environments. Geophys. Res. Lett. 40, 3031–3035.
Dufresne, JL, Foujols, MA, Denvil, S, et al., 2013. Climate change projections using the IPSL-CM5 Earth System Model: From CMIP3 to CMIP5. Clim. Dyn. 40, 2123–2165.
Eyring, V., et al., 2016. Overview of the Coupled Model Intercomparison Project Phase 6 (CMIP6) experimental design and organization. Geosci. Model. Dev. 9, 1937–1958.
Farley, KA, Jobbágy, EG, Jackson, RB, 2005. Effects of afforestation on water yield: A global synthesis with implications for policy. Global Change Biol. 11, 1565–1576.
Fang, J, Chen, A, Peng, C, Zhao, S, Ci, L, 2001. Changes in forest biomass carbon storage in China between 1949 and 1998. Science 292, 2320–2322.
Farquhar, GD, 1997. Carbon dioxide and vegetation. Science 278 1411-1411.
Farrior, CE, Rodriguez-Iturbe, I, Dybzinski, R, Levin, SA, Pacala, SW, 2015. Decreased water limitation under elevated CO_2 amplifies potential for forest carbon sinks. Proc. Natl. Acad. Sci. 112, 7213–7218.
Feng, S, Fu, Q, 2013. Expansion of global drylands under a warming climate. Atmos. Chem. Phys. Discuss. 13, 14637–14665.
Good, S.P., Noone, D., Bowen, G., 2015. Hydrologic connectivity constrains partitioning of global terrestrial water fluxes. Science 349, 175–177.
Grace, J, José, JS, Meir, P, Miranda, HS, Montes, RA, 2006. Productivity and carbon fluxes of tropical savannas. J. Biogeogr. 33, 387–400.
Greve, P, Orlowsky, B, Mueller, B, Sheffield, J, Reichstein, M, Seneviratne, SI, 2014. Global assessment of trends in wetting and drying over land. Nat. Geosci. 7, 716–721.
Greve, P, Seneviratne, SI, 2015. Assessment of future changes in water availability and aridity. Geophys. Res. Lett. 42. doi:10.1002/2015GL064127.
Harper, AB, et al., 2021. Improvement of modeling plant responses to low soil moisture in JULESvn4. 9 and evaluation against flux tower measurements. Geosci. Mod. Dev. 14, 3269–3294.
Held, IM, Soden, BJ, 2006. Robust responses of the hydrological cycle to global warming. J. Clim. 19, 5686–5699.
Hohenegger, C, Brockhaus, P, Bretherton, CS, Schär, C, 2009. The soil moisture–precipitation feedback in simulations with explicit and parameterized convection. J. Clim. 22, 5003–5020.
Hourdin, F, Musat, I, Bony, S, et al., 2006. The LMDZ4 general circulation model: Climate performance and sensitivity to parametrized physics with emphasis on tropical convection. Clim. Dyn. 27, 787–813.
Jackson, RB, Jobbágy, EG, Avissar, R, et al., 2005. Trading water for carbon with biological carbon sequestration. Science 310, 1944–1947.
Jasechko, S, Sharp, ZD, Gibson, JJ, Birks, SJ, Yi, Y, Fawcett, PJ, 2013. Terrestrial water fluxes dominated by transpiration. Nature 496, 347–350.
Kim, Y, Wang, G, 2012. Soil moisture-vegetation-precipitation feedback over North America: Its sensitivity to soil moisture climatology. J. Geophys. Res. Atmos. 117, D18115.
Krinner, G, Viovy, N, De Noblet-Ducoudre, N, et al., 2005. A dynamic global vegetation model for studies of the coupled atmosphere-biosphere system. Global Biogeochem. Cycles 19, GB1015.
Lammertsma, EI, Boer, HJD, Dekker, SC, Dilcher, DL, Lotter, AF, Wagner-Cremer, F, 2011. Global CO_2 rise leads to reduced maximum stomatal conductance in Florida vegetation. Proc. Natl. Acad. Sci. 108, 4035–4040.
Li, Y., et al., 2018. Divergent hydrological response to largescale afforestation and vegetation greening in China. Sci. Adv. 4, eaar4182.
Lian, X, Piao, S, Li, L Z, Li, Y, Huntingford, C, Ciais, P, Cescatti, A, Janssens, IA, Peñuelas, J, Buermann, W, Chen, A, 2020. Summer soil drying exacerbated by earlier spring greening of northern vegetation. Sci. Adv. 6 (1), eaax0255.
Lin, L, Gettelman, A, Feng, S, Fu, Q, 2015. Simulated climatology and evolution of aridity in the 21st century. J. Geophys. Res. Atmos. 120, 5795–5815.
Mahowald, N, Lo, F, Zheng, Y, Harrison, L, Funk, C, Lombardozzi, D, 2015. Leaf area index in Earth System Models: Evaluation and projections. Earth System Dynamics Discussions 6, 761–818.
Mahowald, N, Lo, F, Zheng, Y, Harrison, L, Funk, C, Lombardozzi, D, Goodale, C, 2016. Projections of leaf area index in earth system models. Earth System Dynamics 7, 211–229.
Malhi, Y, Aragão, LEOC, Galbraith, D, et al., 2009. Exploring the likelihood and mechanism of a climate-change-induced dieback of the Amazon rainforest. Proc. Natl. Acad. Sci. 106, 20610–20615.

Marti, O, Braconnot, P, Dufresne, JL, et al., 2010. Key features of the IPSL ocean atmosphere model and its sensitivity to atmospheric resolution. Clim. Dyn. 34, 1–26.
Meng, S, Xie, X, Zhu, B, Wang, Y, 2020. The relative contribution of vegetation greening to the hydrological cycle in the Three-North region of China: A modelling analysis. J. Hydrol. 591, 125689.
Milly, PCD, Dunne, KA, 2010. On the hydrologic adjustment of climate-model projections: The potential pitfall of potential evapotranspiration. Earth Interact. 15, 1–14.
Mueller, B, Seneviratne, SI, 2014. Systematic land climate and evapotranspiration biases in CMIP5 simulations. Geophys. Res. Lett. 41, 128–134.
Notaro, M., Wang, F., Yu, Y., Mao, J., 2020. Projected changes in the terrestrial and oceanic regulators of climate variability across sub-Saharan Africa. Clim. Dyn. 55, 1031–1057.
Penman, HL, 1948. Natural evaporation from open water, bare soil and grass. Proc. R. Soc. Lond. Series A. Math. Phys. Sci. 193, 120–145.
Piao, S, Friedlingstein, P, Ciais, P, De Noblet-Ducoudré, N, Labat, D, Zaehle, S, 2007. Changes in climate and land use have a larger direct impact than rising CO_2 on global river runoff trends. Proc. Natl. Acad. Sci. 104, 15242–15247.
Piao, S, Fang, J, Ciais, P, Peylin, P, Huang, Y, Sitch, S, Wang, T, 2009. The carbon balance of terrestrial ecosystems in China. Nature 458, 1009–1013.
Piao, S, Wang, X, Park, T, Chen, C, Myneni, R B, 2019. Characteristics, drivers and feedbacks of global greening. Nat. Rev. Earth Environ. 1 (1763), 1–14.
Piao, S, Yin, G, Tan, J, et al., 2015. Detection and attribution of vegetation greening trend in China over the last 30 years. Global Change Biol. 21, 1601–1609.
Pielke, RA, Avissar, R, Raupach, M, Dolman, AJ, Zeng, X, Denning, AS, 1998. Interactions between the atmosphere and terrestrial ecosystems: Influence on weather and climate. Global Change Biol. 4, 461–475.
Poulter, B, Frank, D, Ciais, P, et al., 2014. Contribution of semi-arid ecosystems to interannual variability of the global carbon cycle. Nature 509, 600–603.
Rahman, MM, Lu, M, Kyi, KH, 2015. Variability of soil moisture memory for wet and dry basins. J. Hydrol. 523, 107–118.
Rebel, KT, De Jeu, RM, Ciais, P, Viovy, N, Piao, SL, Kiely, G, Dolman, AJ, 2012. A global analysis of soil moisture derived from satellite observations and a land surface model. Hydrol. Earth Syst. Sci. 16, 833–847.
Rihani, JF, Chow, FK, Maxwell, RM, 2015. Isolating effects of terrain and soil moisture heterogeneity on the atmospheric boundary layer: Idealized simulations to diagnose land-atmosphere feedbacks. J. Adv. Model. Earth Syst. 7, 915–937.
Robert, BJ, James, TR, Josep, GC, et al., 2008. Protecting climate with forests. Environ. Res. Lett. 3, 044006.
Robock, A, Vinnikov, KY, Srinivasan, G, et al., 2000. The global soil moisture data bank. Bull. Am. Meteorol. Soc. 81, 1281–1299.
Roderick, ML, Greve, P, Farquhar, GD, 2015. On the assessment of aridity with changes in atmospheric CO_2. Water Resour. Res. 51. doi:10.1002/2015WR017031.
Roth, N, et al., 2021. A call for consistency with the terms' wetter'and 'drier' in climate change studies. Environ. Evid. 10, 1–7.
Schimel, D, Stephens, BB, Fisher, JB, 2015. Effect of increasing CO_2 on the terrestrial carbon cycle. Proc. Natl. Acad. Sci. 112, 436–441.
Seager, R, Vecchi, GA, 2010. Greenhouse warming and the 21st century hydroclimate of southwestern North America. Proc. Natl. Acad. Sci. 107, 21277–21282.
Segal, M, Arritt, RW, Clark, C, Rabin, R, Brown, J, 1995. Scaling evaluation of the effect of surface characteristics on potential for deep convection over uniform terrain. Month. Weath. Rev. 123, 383–400.
Segal, M, Garratt, JR, Kallos, G, Pielke, RA, 1989. The impact of wet soil and canopy temperatures on daytime boundary–layer growth. J. Atmospheric Sci. 46, 3673–3684.
Sellar, AA, Walton, J, Jones, CG, Wood, R, Abraham, N L, Andrejczuk, M, Andrews, MB, Andrews, T, Archibald, A.T, de Mora, L, Dyson, H, 2020. Implementation of UK Earth system models for CMIP6. J. Adv. Model. Earth Syst. 12 (4) e2019MS001946.
Seneviratne, SI, 2012. Climate science: Historical drought trends revisited. Nature 491, 338–339.
Seneviratne, SI, Luthi, D, Litschi, M, Schar, C, 2006. Land-atmosphere coupling and climate change in Europe. Nature 443, 205–209.
Sheffield, J, Wood, EF, Roderick, ML, 2012. Little change in global drought over the past 60 years. Nature 491, 435–438.
Sherwood, S, Fu, Q, 2014. A drier future? Science 343, 737–739.
Spracklen, DV, Arnold, SR, Taylor, CM, 2012. Observations of increased tropical rainfall preceded by air passage over forests. Nature 489, 282–285.
Stocker, TF, Qin, D, Plattner, GK, et al., 2013. Climate change 2013 the physical science basis: Contribution of working group I to the fifth assessment report of the IPCC. Cambridge University Press, New York, USA.
Swann, ALS, Fung, IY, Chiang, JCH, 2012. Mid-latitude afforestation shifts general circulation and tropical precipitation. Proc. Nat. Acad. Sci. U.S.A. 109, 712–716.
Taylor, KE, Stouffer, RJ, Meehl, GA, 2012. An overview of CMIP5 and the experiment design. Bull. Am. Meteorol. Soc. 93, 485–498.
Thomson, A, Calvin, K, Smith, S, et al., 2011. RCP4.5: A pathway for stabilization of radiative forcing by 2100. Clim. Change 109, 77–94.
Trenberth, KE, Dai, A, Van Der Schrier, G, Jones, PD, Barichivich, J, Briffa, KR, Sheffield, J, 2013. Global warming and changes in drought. Nat. Clim. Change 4, 17–22.
Yu, L, Xue, Y, Diallo, I, 2021. Vegetation greening in China and its effect on summer regional climate. Sci. Bull. 66 (1), 13–17.
Zeng, Z, Piao, S, Chen, A, Lin, X, Nan, H, Li, J, Ciais, P, 2013. Committed changes in tropical tree cover under the projected 21st century climate change. Sci. Rep. 3. doi:10.1038/srep01951.
Zeng, Z., et al., 2017. Climate mitigation from vegetation biophysical feedbacks during the past three decades. Nat. Clim. Change 7, 432–436.
Zeng, Z., et al., 2018. Impact of Earth greening on the terrestrial water cycle. J. Clim. 31, 2633–2650.
Zhang, K, Kimball, JS, Nemani, RR, Running, SW, Hong, Y, Gourley, JJ, Yu, Z, 2015. Vegetation greening and climate change promote multidecadal rises of global land evapotranspiration. Sci. Rep. 5, 15956.
Zhou, L, Tucker, CJ, Kaufmann, RK, Slayback, D, Shabanov, NV, Myneni, RB, 2001. Variations in northern vegetation activity inferred from satellite data of vegetation index during 1981 to 1999. J. Geophys. Res. 106, 20069–20083.
Zhu, Z, Bi, J, Pan, Y, et al., 2013. Global data sets of vegetation leaf area index (LAI) 3g and Fraction of Photosynthetically Active Radiation (FPAR) 3g derived from Global Inventory Modeling and Mapping Studies (GIMMS) Normalized Difference Vegetation Index (NDVI3g) for the period 1981 to 2011. Rem. Sens. 5, 927–948.
Zhu, Z, Piao, SL, Myneni, RB, et al., 2016. Greening of the Earth and its drivers. Nat. Clim. Change doi:10.1038/nclimate3004.

Jie Wu received her B.S. and M.S. degrees from Hohai University in 2015 and 2019, respectively. She is currently a Ph.D. student of the Collaborative Ph.D. Programs between the University of Copenhagen and the Southern University of Science and Technology. Her research work focuses on the biophysical feedback from earth greening.

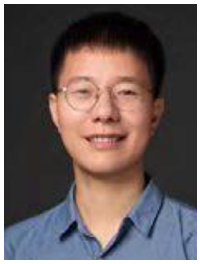

Zhenzhong Zeng received his B.S. degree from Sun-Yet Sen University in 2011, and Ph.D. degree from Peking University in 2016. He led a tropical deforestation project at Princeton University during 2016-2019. Since 2019, he led a lab on Earth system and global change, with a focus on global climate change and its natural-based solutions.